Interactive Visualization of the Coupler Surfaces of the Spatial 4C Mechanism

Pierre M. Larochelle
e-mail: pierrel@fit.edu

Agnes M. Agius

Mechanical & Aerospace Engineering
Department,
Florida Institute of Technology, Melbourne, FL

This paper presents a methodology for generating and displaying the coupler surfaces of the spatial 4C mechanism. The 4C mechanism is a two-degree-of-freedom spatial four-bar linkage. The path traced by a point attached to the coupler or floating link defines a surface in space. It is shown that the coupler surface of the spatial 4C mechanism is a ruled surface with 16th degree *directrices. An interactive graphical user interface has been created and integrated with kinematic analysis routines to generate and interactively display these coupler surfaces. The result is a user-friendly and efficient means of generating and visualizing the coupler surfaces of the spatial 4C four-bar mechanism.* [DOI: 10.1115/1.2049067]

1 Introduction

In this paper we present a parametrized representation of the coupler surface of the general spatial 4C four-bar mechanism (see see Fig. 1) devised to facilitate interactive visualization. The methodology utilizes an analytic representation of the linkage's coupler point position that is parametrized by the mechanism's joint variables (i.e., rotation angles and translational distances). The kinematic analysis of the kinematic closed chain is utilized to eliminate all but two joint variables. The result is a representation of the coupler surface associated with a coupler point on a spatial four-bar mechanism that is parametrized by its two driving joint variables.

Recently, there have been some significant efforts made to address the challenge of designing useful spatial mechanisms. A novel idea of serially coupling spatial joints to facilitate the generation of spatial motion was presented in [1]. In [2], a Burmester-Theory-based computer-aided design program for spatial 4C mechanisms was reported. Efforts were made to address circuit and branch defects in [3]. Approximate motion synthesis was addressed in [4] and [5], whereas function generation has been address in [6]. Point paths of the RCCC mechanism were studied in [7], and the design of these mechanisms to avoid jamming movements was addressed in [8]. The invariant properties of the motions that spatial mechanisms generate has been studied in [9]. A study of the effects of joint clearance in spatial mechanisms is reported in [10]. The exploration of utilizing virtual reality techniques to address the inherent visualization and interaction challenges was reported in [11]. The design of a passively balanced spatial linkage for use in a haptic interface was presented by [12]. A study of fabrication errors in the manufacture of spatial mechanisms was reported in [13]. Moreover, the work reported here was motivated to a large extent by the study of the coupler curves of the RCCC mechanism reported by Marble and Pennock in [14]. They used a dual-number approach to generate parametric equations of the coupler curves of RCCC spatial four-bar mechanisms. Furthermore, Marble and Pennock proved that the polynomial describing the coupler curve is 16th degree. Here, we build upon their work and examine the coupler surfaces of the 4C mechanism.

The immediate goal here was to perform a kinematic study of the coupler surfaces of the spatial 4C mechanism and to create an interactive visualization tool to present these surfaces. This is one step toward the long-term goal of creating an interactive computer-aided-design software tool to synthesize spatial 4C mechanisms for prescribed coupler surfaces. Such mechanisms would be applicable wherever complex surface motions are required and/or manufactured; such as in free-form modeling and manufacturing, mold and pattern making, surface finishing, etc. Consider this conceptual example of free-form manufacturing, a NURBS-based software (e.g., Alias' SurfaceStudio™ or McNeel & Associates' Rhinoceros™) could be used to design and prescribe a desired complex free-form surface. A spatial 4C mechanism could then be synthesized such that its coupler surface includes the prescribed surface. Finally, the free-form surface could be manufactured via material removal from raw stock by attaching a cutting tool to the coupler of the mechanism such that the tip of a cutting tool is coincident with the coupler point. See [15] for a study of the rapid-prototyping manufacturability of ruled surfaces. Let us consider another conceptual example, the design and manufacture of a complex automobile quarter panel. These surfaces are often generated with free-form surface-design software programs. A spatial 4C mechanism could be designed such that its coupler point traces the prescribed surface. Such a mechanism could be applicable to (1) making the patterns/dies used to manufacture the quarter panels, (2) surface finishing of the quarter panels (grinding, sanding, painting, etc.), and, (3) inspecting the finished quarter panels (e.g., cameras, touch probes, etc.). In 2001, [16] proposed a framework for the interactive design of rigid-body motions. Here, one could envision future work to address interactive design of spatial mechanism for desired coupler surfaces.

The paper proceeds as follows. First, the necessary kinematic analyses of the spatial 4C mechanism are performed. Next, we utilize the results of this analysis to reveal the properties and structure of the coupler surface. We continue by utilizing the results of the analyses to generate the parametric representation of the coupler surface of the spatial 4C mechanism. Finally, the interactive visualization program *SPASUR* (spatial surfaces) [17] is used to present images of example coupler surfaces.[1]

2 Spatial 4C Mechanism

A spatial 4C mechanism has four cylindrical or C joints, each joint permitting relative rotation and translation along a line, see Fig. 1. These four C joints connect four rigid bodies to form a

---

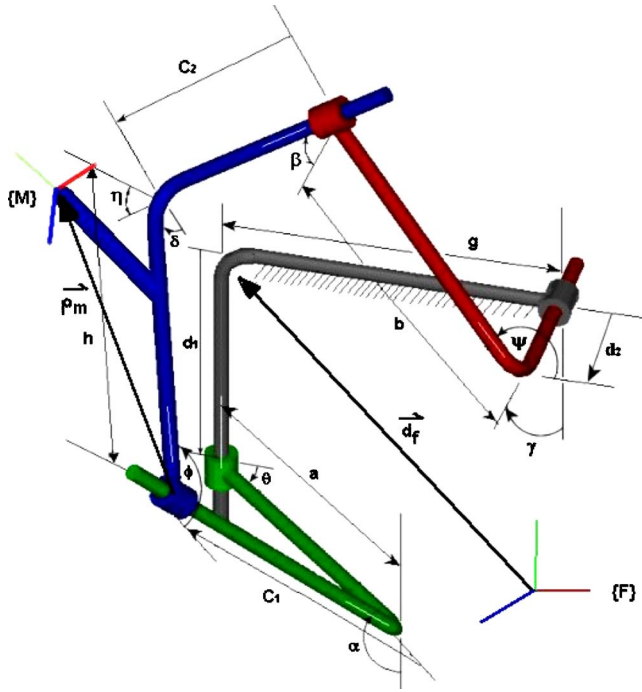[1]Source code for *SPASUR* is available on request from the author.

Fig. 1 Spatial 4C mechanism

spatial closed chain. The link parameters that define the mechanism are listed in Table 1, and the joint variables are defined in Table 2.

The spatial 4C mechanism may be viewed as a combination of two CC dyads where each dyad connects the coupler to the fixed or ground link. The driving or input CC dyad has four independent joint variables, referred to as θ, d_1, ϕ, and c_1. The driven or output dyad also has four independent joint variables, ψ, d_2, δ, and c_2. When adjoined by the coupler link, the two dyads form a closed-chain spatial 4C mechanism with two degrees of freedom. We chose θ and d_1 to be the independent driving joint variables. Note that ϕ and c_1 as well as the driven dyad's joint variables are now explicit functions of θ and d_1 and these functions are found below.

2.1 Spatial 4C Mechanism Analysis We now present the equations that define the relative movement for the links of a spatial 4C mechanism given its physical dimensions and the input variable, θ and d_1. The closed-chain vector loop equations were solved to yield the following equations (see [2,18,19]).

The coupler angle ϕ as a function of the input angle θ is

Table 1   Link parameters of the spatial 4C mechanism

Link	Twist	Length
Driving	α	a
Coupler	η	h
Driven	β	b
Fixed	γ	g

Table 2   Joint variables of the spatial 4C mechanism

Joint	Rotation	Translation
Driving fixed	θ	d_1
Driving moving	ϕ	c_1
Driven moving	δ	c_2
Driven fixed	ψ	d_2

$$\phi(\theta) = \arctan\left(\frac{B}{A}\right) \pm \arccos\left(\frac{C}{\sqrt{A^2 + B^2}}\right) \quad (1)$$

where

$$A = \sin(\eta)\sin(\gamma)\cos(\alpha)\cos(\theta) - \sin(\alpha)\sin(\eta)\cos(\gamma)$$

$$B = -\sin(\eta)\sin(\gamma)\sin(\theta)$$

$$C = \cos(\beta) - \cos(\eta)\sin(\alpha)\sin(\gamma)\cos(\theta) - \cos(\alpha)\cos(\eta)\cos(\gamma)$$

Note that ϕ has two solutions corresponding to the two assemblies or circuits of the mechanism.

The output angle ψ as a function of the input angle θ and the coupler angle ϕ is

$$\psi(\theta, \phi) = \arctan\left(\frac{B}{A}\right) \quad (2)$$

where

$$A = \frac{1}{-\sin(\beta)}\{\cos(\eta)[\cos(\alpha)\sin(\gamma) - \cos(\gamma)\cos(\theta)\sin(\alpha)]$$
$$- \sin(\eta)\cos(\phi)[\cos(\alpha)\cos(\gamma)\cos(\theta) + \sin(\alpha)\sin(\gamma)]$$
$$+ \sin(\eta)\cos(\gamma)\sin(\phi)\sin(\theta)\}$$

$$B = \frac{1}{\sin(\beta)}\{\cos(\eta)\sin(\alpha)\sin(\theta) + \sin(\eta)\cos(\theta)\sin(\phi)$$
$$+ \sin(\eta)\cos(\alpha)\cos(\phi)\sin(\theta)\}$$

The output coupler angle δ (i.e., the angle between the coupler and driven link) is

$$\delta(\theta, \psi) = \arctan\left(\frac{B}{A}\right) \quad (3)$$

where

$$A = \frac{1}{\sin(\eta)}\{\cos(\alpha)[\cos(\gamma)\sin(\beta) + \cos(\beta)\sin(\gamma)\cos(\psi)]$$
$$- \sin(\alpha)\cos(\theta)[\cos(\beta)\cos(\gamma)\cos(\psi) - \sin(\beta)\sin(\gamma)]$$
$$- \sin(\alpha)\cos(\beta)\sin(\theta)\sin(\psi)\}$$

$$B = \frac{1}{-\sin(\eta)}\{\cos(\alpha)\sin(\gamma)\sin(\psi) + \sin(\alpha)\sin(\theta)\cos(\psi)$$
$$- \sin(\alpha)\cos(\gamma)\cos(\theta)\sin(\psi)\}$$

Finally, the driving coupler translation c_1, the translation along the driving moving axis, is given by

$$c_1(\theta, \psi, \delta, d_1) = \frac{A}{B} \quad (4)$$

where

$$A = d_1\sin(\gamma)\sin(\psi) + a\cos(\theta)\cos(\psi) + a\cos(\gamma)\sin(\theta)\sin(\psi)$$
$$+ h\cos(\delta) - b - g\cos(\psi)$$

$$B = \sin(\eta)\sin(\delta)$$

2.2 Mechanism Classification. In order to understand the characteristics of the coupler surface and to facilitate its visual representation, it is necessary to know the mechanism's classification or type. In the case of spatial 4C mechanisms, the angular relationships define the gross motion characteristics and we therefore employ the spherical image classification scheme of Murray and Larochelle [20]. Duffy [18] shows that there is a spherical image associated with each spatial four-bar mechanism. The spherical image is a spherical 4R mechanism having link lengths equal to the angular twists of the 4C mechanism $(\alpha, \gamma, \eta, \beta)$, see
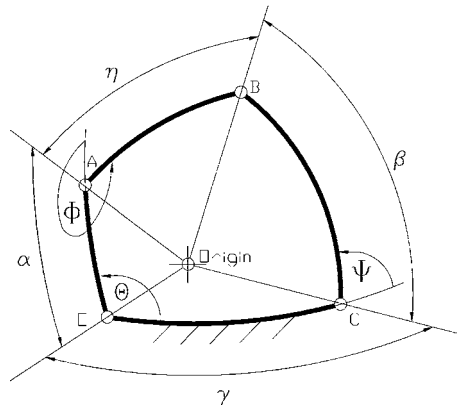
Fig. 2 Spherical four-bar image

Fig. 2. We utilize the following parameters, introduced in [20], to classify the spherical image of a spatial 4C mechanism

$$T_1 = \gamma - \alpha + \eta - \beta$$

$$T_2 = \gamma - \alpha - \eta + \beta$$

$$T_3 = \eta + \beta - \gamma - \alpha$$

$$T_4 = 2\pi - \eta - \beta - \gamma - \alpha$$

The four parameters T_i, $i = 1, 2, 3, 4$ classify the movement of the driving and driven links of the spherical $4R$ linkage into 16 basic types (see Table 3). In this table the classification of non-Grashof mechanisms includes a preceding pair of numbers that denote the rocking range of motion of the input and output links. The first number refers to the input link angle θ and the second to the output link angle ψ, where a 0 indicates that the rocking range includes the angle 0 and a π indicates that the range includes the angle π. The $\pm$ that follows these numbers indicates the algebraic sign of the T_4 parameter for the mechanism type. Moreover, in terms of these T parameters, the Grashof condition for spherical $4R$ mechanisms may be stated as $T_1 T_2 T_3 T_4 > 0$. If the Grashof condition is satisfied, then one or more links can fully rotate and the mechanism has two distinct assemblies. Most importantly, for each different assembly of a 4C mechanism, a distinct and separate coupler surface exists.

2.2.1 Range of Motion Analysis. Because we are using a representation of the coupler surface that is parametrized by the driving link's rotation (θ) and translation (d_1) with respect to the fixed

link, we now seek to determine the valid ranges for these input variables for a general spatial 4C mechanism. Knowing these ranges facilitates the generation of the coupler surfaces. The driving link's range of motion depends on the mechanism's link parameters. Moreover, the shape of the coupler surfaces is related to this classification. We can decern four distinct types of ranges for the rotational motion of the driving link; however, the translational motion of the driving link does not have any inherent limits. Although in practice, the joint axes must be of finite length and, if known, these limits may be imposed when generating the coupler surfaces. Considering the spherical image of a 4C spatial mechanism shown in Fig. 2, the relationship between the input angle θ of the driving link to the output angle ψ of the driven link is

$$\psi(\theta) = \arctan\left(\frac{B}{A}\right) \pm \arccos\left(\frac{C}{\sqrt{A^2 + B^2}}\right) \quad (5)$$

where

$$A(\theta) = \sin(\alpha)\sin(\beta)\cos(\gamma)\cos(\theta) - \cos(\alpha)\sin(\beta)\sin(\gamma)$$

$$B(\theta) = \sin(\alpha)\sin(\beta)\sin(\theta)$$

$$C(\theta) = \cos(\eta) - \cos(\alpha)\cos(\beta)\cos(\gamma) - \sin(\alpha)\cos(\beta)\sin(\gamma)\cos(\theta)$$

and $0 \leq \alpha, \beta, \eta, \gamma \leq \pi$.

The argument to the arccos ( ) function in Eq. (5) must be in the range -1–1 for a solution to exist. Therefore, we can write $A(\theta)^2 + B(\theta)^2 - C(\theta)^2 \geq 0$, and we can use this relation to determine the range of the angular movement of the input link. Expanding this inequality yields a quadratic equation in $\cos(\theta)$ that has two roots $C_1 = \cos(\theta_1)$ and $C_2 = \cos(\theta_2)$, where $\theta_1 \leq \theta_2$ and

$$C_1 = \frac{\cos(\eta - \beta) - \cos(\alpha)\cos(\gamma)}{\sin(\alpha)\sin(\gamma)}$$

$$C_2 = \frac{\cos(\eta + \beta) - \cos(\alpha)\cos(\gamma)}{\sin(\alpha)\sin(\gamma)}$$

These equations define the θ limits and, therefore, the range of rotational motion of the driving link. These limiting angles exist if $-1 < C_1$ or $C_2 < 1$. There are four possible cases:

1. Neither of the limiting angles θ_1 or θ_2 exists; hence, the input link fully rotates.
2. Only $\theta_1 = \arccos(C_1)$ exists; hence, the input link rocks through the angle $\theta = \pi$ between $\pm \theta_1$.
3. Only $\theta_2 = \arccos(C_2)$ exists; hence, the input link rocks through the angle $\theta = 0$ between $\pm \theta_2$.

Table 3 Basic spherical 4R linkage types

	Linkage type	T_1	T_2	T_3	T_4
1.	Crank-rocker	+	+	+	+
2.	Rocker-crank	+	−	−	+
3.	Double-crank	−	−	+	+
4.	Grashof double-rocker	−	+	−	+
5.	00+ double-rocker	−	−	−	+
6.	$0\pi+$ double-rocker	+	+	−	+
7.	$\pi 0+$ double-rocker	+	−	+	+
8.	$\pi\pi+$ double-rocker	−	+	+	+
9.	Crank-rocker	−	−	−	−
10.	Rocker-crank	−	+	+	−
11.	Double-crank	+	+	−	−
12.	Grashof double-rocker	+	−	+	−
13.	00− double-rocker	+	+	+	−
14.	$0\pi-$ double-rocker	−	−	+	−
15.	$\pi 0-$ double-rocker	−	+	−	−
16.	$\pi\pi-$ double-rocker	+	−	−	−

Table 4 Input link rotational motion ranges

Mechanism type	Input link motion	θ range
Crank rocker or double crank	Fully rotates	0 to 2π
Double rocker or rocker crank	Two ranges	θ_1 to θ_2 and $-\theta_1$ to $-\theta_2$
00 or 0π double rocker	Rocks through 0	$-\theta_2$ to θ_2
$\pi0$ or $\pi\pi$ double rocker	Rocks through π	θ_1 to $-\theta_1$

4. Both angles exist; hence, the input rocks between θ_1 and θ_2 and $-\theta_1$ and $-\theta_2$ and does not pass through either 0 or π.

In the classification above, the first two cases correspond to Grashof mechanisms and the last two to non-Grashof mechanisms. Table 4 summarizes the foregoing analyses.

3 Parametrized Coupler Surface

We now utilize the solution of the kinematic analysis to derive a parametrized representation of the coupler surface associated with a spatial 4C mechanism. First, we generate a representation of a prescribed coupler point $\vec{p}$ that is parametrized by the driving joint variables θ and d_1. This is done by performing a forward kinematic analysis of the driving dyad,

$$\vec{p}(\theta, d_1) = FZ(\theta, d_1)X(\alpha, a)Z(\phi, c_1)\vec{p}_M \qquad (6)$$

where Fig. 3 illustrates the sequence of transformations, $\vec{p}_M$ is the coupler point expressed with respect to the moving frame attached to the coupler link, and F is the homogeneous transform from the fixed reference frame to the frame attached to the fixed link. Equation (6) yields the coupler surface of the spatial 4C mechanisms parametrized by the two driving joint variables θ and d_1, since $\phi(\theta)$ and $c_1(\theta, d_1)$ are given by Eqs. (1) and (4), respectively.

4 Properties of the Coupler Surface

In this section we seek identify the properties of the coupler surfaces of the spatial 4C mechanism that facilitate its interactive visualization.

4.1 Number of Coupler Surfaces. The discussion above regarding classifying the spatial 4C mechanism into 16 distinct types based on its spherical image revealed that Grashof 4C mechanisms (i.e., those with $T_1T_2T_3T_4 > 0$) will have two distinct assemblies or circuits, whereas non-Grashof mechanisms will have one assembly. Each assembly or circuit of the spherical im-age has a unique coupler curve, and each coupler curve of the spherical image corresponds to a coupler surface of the associated spatial 4C mechanism. Hence, Grashof 4C mechanisms will have two distinct coupler surfaces, whereas non-Grashof mechanisms will have one.

4.2 Structure of Coupler Surfaces. The kinematic analysis of the 4C mechanism presented above was done such that the independent or driving variables are the input angle θ and the input translation d_1, which locate the driving link with respect to the fixed link. By holding θ constant, these equations yield the analysis of the resulting spatial PCCC mechanism whose input is the translation d_1. Note furthermore that by holding θ constant that all of the angular relationships (i.e., ϕ, δ, and ψ) will be constant and, hence, the PCCC mechanism will, in fact, have the mobility and motion characteristics of this corresponding 4P mechanism.

The 4P mechanism has one degree of freedom, and therefore, the path traced by a coupler point yields a coupler curve. A parametric representation of the coupler curve of the PCCC mechanism can be be obtained by using Eq. (6), while holding θ constant. However, it is clear that since the angular relationships are constant in the 4P mechanism, the coupler curve must be a straight line. Sample coupler curves (i.e., lines) of a 4P mechanism for 36 different values of θ are shown in Fig. 4.

In a similar manner, we examine the coupler curves that result from fixing the other driving variable (d_1) of the 4C mechanism. The result of holding constant the input translation d_1 is a one degree of freedom RCCC mechanism. Marble and Pennock in [14] used a dual-number approach and proved that the polynomial describing this coupler curve is 16th degree. A parametric representation of the coupler curve of the RCCC mechanism can be obtained by using Eq. (6), while holding d_1 constant. Sample coupler curves of an RCCC mechanism for 11 different values d_1 are shown in Fig. 5.

The two-degree-of-freedom 4C mechanism has a coupler surface that is a combination of its associated 4P and RCCC coupler
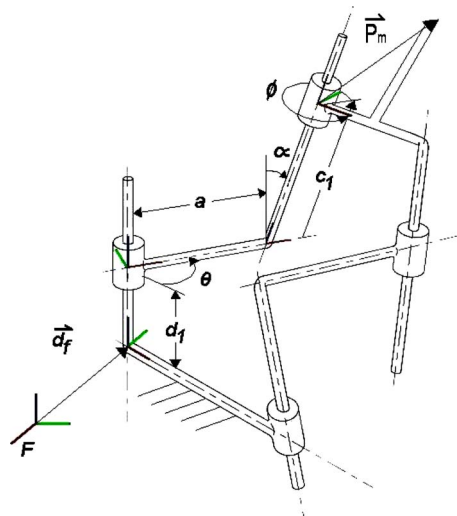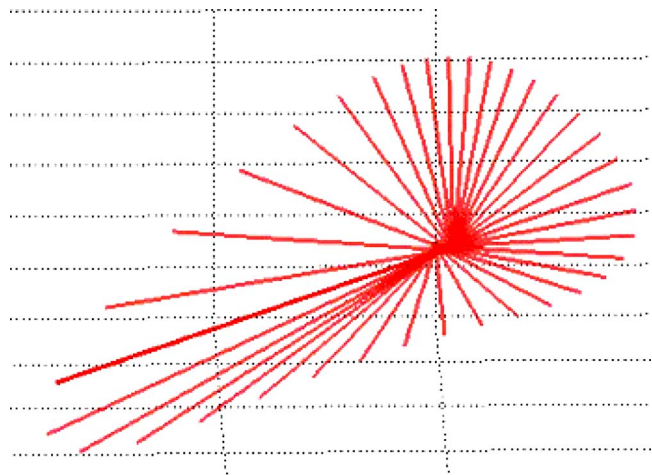

Fig. 3 Forward kinematic analysis
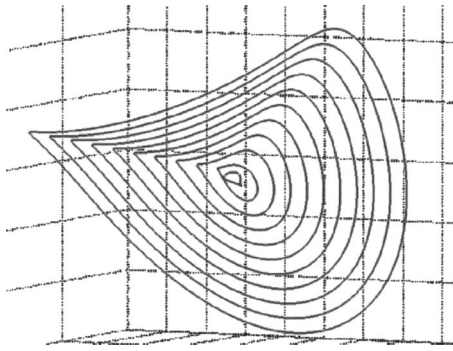

Fig. 4 Sample spatial PCCC coupler curves

Fig. 5 Sample spatial RCCC coupler curves

Fig. 7 Spatial 4C crank-rocker coupler surfaces

curves. Moreover, because the coupler curve of the 4P mechanism is a straight line, we conclude that the coupler surface of the spatial 4C mechanisms is a ruled surface (see [21] for a discussion of ruled surfaces). Hence, the coupler surface of a 4C mechanism is a ruled surface, where the 16th degree closed coupler curve of the associated RCCC mechanism serves as its directrix or base curve and the rulings or lines are the coupler curves of the associated 4P mechanism.

4.3 Coupler Surfaces With Singular Regions. In [9] it is shown that non-Grashof mechanisms encounter translational singular configurations when their input angle θ reaches the boundaries of its valid range; see also [22] for supplementary discussions of these translational singular configurations. In these translational singular configurations $\delta = 0$ or π, which results in $c_1 \rightarrow \pm\infty$ [see Eq. (4)]. Furthermore, when $c_1 \rightarrow \pm\infty$, we have, from Eq. (6), that points $\vec{p}$ on the coupler surface will approach $\pm\infty$. Hence, the coupler surface associated with a non-Grashof 4C mechanism has singular regions (or regions that approach infinity), which correspond to when the input angle θ reaches the limits of its valid range of motion.

There exists one degenerate case that needs to be addressed. Foster and Cipra [22] show that there exists one specific value of d_1 such that when $\delta = 0$ or π, c_1 can take on any finite value. We consider this too to be a translational singular configuration since fixing d_1 to a specific value degenerates the couple surface to a specific directrix (i.e., the coupler curve of a specific RCCC mechanism). Moreover, the methodology presented in Sec. 5 for generating the parametrized representation of the coupler surface yields these degenerate coupler curves as directrices. Hence, a spatial 4C mechanism that enters such a special configuration will have its coupler point trace out a specific directrix on this coupler surface. As such, no additional work is needed to address this degenerate case.
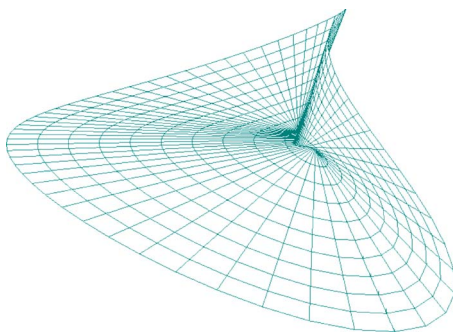
5 SPASUR

In this section we present *SPASUR* and visualizations of two example coupler surfaces. First, the analysis methodologies presented above were programed using MATLAB-7, and a simple and efficient user interface was designed, see Figs. 9 and 12. The user interface allows for both the direct entry of numerical data and/or the use of slider bars to permit parametric design studies.

The coupler surfaces are generated by discretizing the range of input translational motion d_1 over a prescribed finite range; in the examples presented here $0 \leq d_1 \leq 100$. For each value of d_1, we vary θ through its allowable range of motion using the mechanism classification scheme and analyses presented above to determine the mechanism's type and valid θ range(s). We have found it useful to provide the user a means of controlling the step sizes $\Delta\theta$ and Δd_1 of the discretization because larger step sizes result in faster generation of the coupler surfaces and smaller ones yield increased resolution of the coupler surface details. For each driving joint variable pair (θ, d_1), we generate the four vertices $(\vec{v})$ and their associated normals $(\vec{n})$ of a quadrilateral graphics primitive by using Eq. (6) as follows:

$$\vec{v}_1 = \vec{p}(\theta, d_1)$$
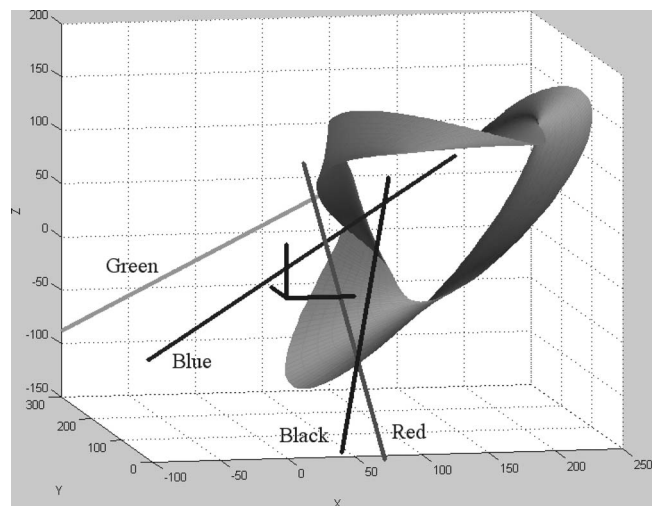
$$\vec{v}_2 = \vec{p}(\theta, d_1 + \Delta d_1)$$

Fig. 6 Quadrilateral primitives used to render the coupler surfaces

Fig. 8 Spatial 4C crank-rocker: One coupler surface with joint axes

Fig. 9   Crank-rocker mechanism data and user interface
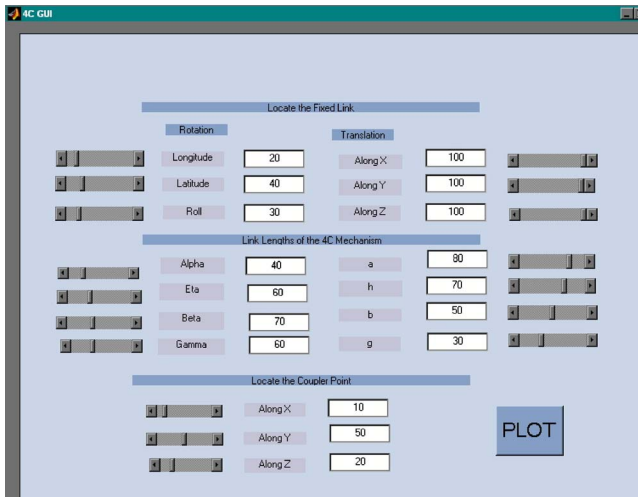
Fig. 10   Spatial 4C double-rocker coupler surface

$$\vec{v}_3 = \vec{p}(\theta + \Delta\theta, d_1 + \Delta d_1)$$

$$\vec{v}_4 = \vec{p}(\theta + \Delta\theta, d_1)$$

$$\vec{n}_1 = (\vec{v}_4 - \vec{v}_1) \times (\vec{v}_2 - \vec{v}_1)$$

$$\vec{n}_2 = (\vec{v}_1 - \vec{v}_2) \times (\vec{v}_3 - \vec{v}_2)$$

$$\vec{n}_3 = (\vec{v}_2 - \vec{v}_3) \times (\vec{v}_4 - \vec{v}_3)$$

$$\vec{n}_4 = (\vec{v}_3 - \vec{v}_4) \times (\vec{v}_1 - \vec{v}_4)$$

In this formulation, vertices $\vec{v}_1$ and $\vec{v}_2$ lie on one ruling and vertices $\vec{v}_3$ and $\vec{v}_4$ lie on a neighboring ruling. Moreover, vertices $\vec{v}_1$ and $\vec{v}_4$ lie on one directrix or base curve and vertices $\vec{v}_2$ and $\vec{v}_3$ lie on a neighboring directrix. Figure 6 shows the sides of the quadrilaterals generated to represent a coupler surface. Finally, MATLAB-6 provides the user with efficient means for interactive visualization of the surfaces, including rotating view functions, scaling, and surface rendering, and lighting.

5.1   Spatial 4C Crank-Rocker Mechanism. The coupler surfaces associated with a crank-rocker spatial 4C mechanism are shown in Figs. 7 and 8. Because this is a Grashof mechanism, there are two distinct coupler surfaces associated with it, as shown in Fig. 7. In Fig. 8, one of the coupler surfaces is shown as well as the joint axes of the spatial 4C mechanism; *black*=driving fixed axis, *green*=driving moving axis, *red*=driven moving axis, and *blue*=driven fixed axis. The data for this mechanism is found in Fig. 9.

5.2   Spatial 4C Double-Rocker Mechanism. The coupler surface associated with a $\pi\pi+$ double-rocker spatial 4C mechanism is shown in Fig. 10. This is a non-Grashof mechanism, and there is only one associated coupler surface. Note that this mechanism reaches translational singular configurations at the limits of its θ motion (see [3,22]). In these translational singular configurations, $\delta=0$ or π, which results in $c_1 \rightarrow \pm\infty$ [see Eq. (4)]. The resulting effect is the *planar* appearing region of the coupler surface. This region is not real and only appears because the points on the coupler surface approach $\pm\infty$. In Fig. 11, the coupler surface is shown again, but here the driving angle θ has been bounded to remain 15 deg away from the limits of its range of motion. Note that by doing so the mechanism avoids the translational singular configurations that occur at the θ limits; see [3] for further discussion of the translational singular configurations of the 4C mechanism. The data for this mechanism is found in Fig. 12.
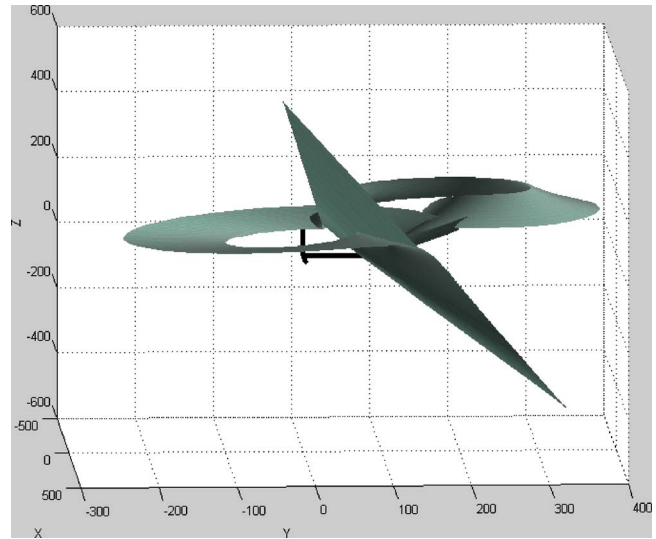
5.3   Immersive VR Representation. Recent efforts by Vance and Larochelle [23] have sought to employ the visualization capabilities of immersive virtual reality to facilitate the design of spatial mechanisms. In Fig. 13, is shown a visualization of a pair of coupler surfaces in the immersive *C*6 facility at Iowa State University. Preliminary results indicate that visual representation of the coupler surfaces has proven to be useful when designing spatial 4C mechanisms using the VRSpatial design software [11]. VRSpatial was developed by a team of researchers lead by Professor Larochelle, at the Florida Institute of Technology, and Professor Vance, at the Iowa State University.

6   Conclusions

This paper has presented the study of the coupler surfaces of the spatial 4C mechanism. The results are that the coupler surface of a spatial 4C mechanism is a ruled surface with 16th degree directrices and straight lines as generators. The directrices are the coupler curves of the associated RCCC mechanism, and the straight lines are the coupler curves of the associated PCCC (or 4P) mechanism. Parametric equations for the coupler surface are
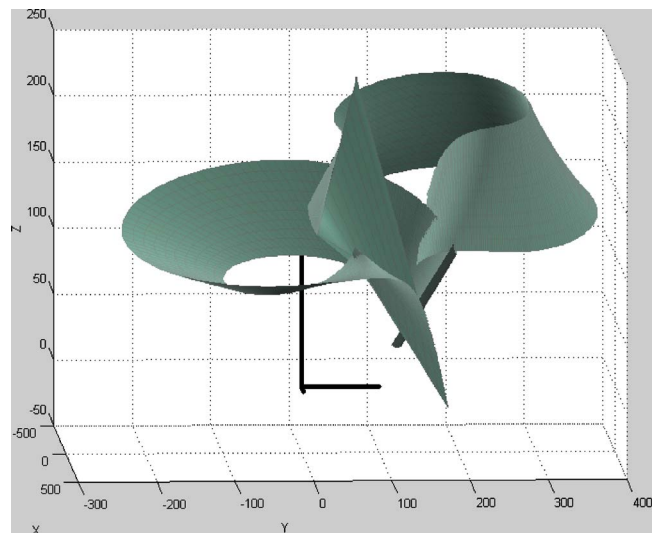

Fig. 11   Spatial 4C double-rocker coupler surface: Modified θ range
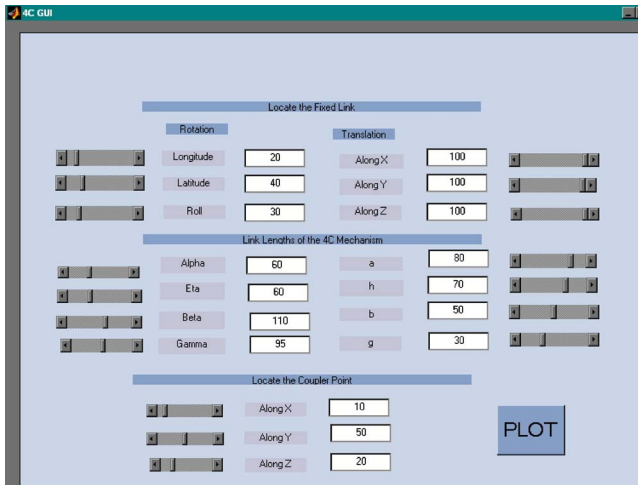
Fig. 12 Double-rocker mechanism data and user interface

Fig. 13 Virtual reality representation of a coupler surface

derived, and the closed kinematic chain constraints on the two degrees of freedom of the mechanism are addressed. Moreover, a software tool entitled *SPASUR* (spatial surface), for the interactive visualization of the coupler surfaces of the spatial 4C mechanism, has been discussed. An interactive graphical user interface has been created and integrated with kinematic analysis routines to generate and display these coupler surfaces. The result is a user-friendly and efficient means of generating and visualizing the coupler surfaces of the spatial 4C four-bar mechanism. This is one step toward the long-term goal of creating an interactive computer-aided-design software tool to synthesize spatial 4C mechanisms for prescribed coupler surfaces.

Acknowledgments

References

[1] Krovi, V., Aranthasurech, G. K., and Kumar, V., 2001, "Kinematic and Kine-tostatic Synthesis of Planar Coupled Serial Chains," J. Mech. Des., **123**(3), pp. 359–366.
[2] Larochelle, P., 1998, "SPADES: Software for Synthesizing Spatial 4c Mecha-nisms," *Proc. of ASME Design Engineering Technical Conference*, Atlanta, ASME, New York.
[3] Larochelle, P., 2000, "Circuit and Branch Rectification of the Spatial 4c Mechanism," *Proc. of ASME Design Engineering Technical Conference*, Bal-timore, ASME, New York.
[4] Larochelle, P., 1994, "Design of Cooperating Robots and Spatial Mecha-nisms," Ph.D. Dissertation, University of California, Irvine.
[5] Larochelle, P., and Dees, S. L., 2002, "Approximate Motion Synthesis Using an SVD-Based Distance Metric," *Proc. of 8th International Symposium on Advances in Robot Kinematics (ARK)*, Caldes de Malavella, Spain, June 24–28, Kluwer Academic Publishers, Dordrecht, Boston, London, pp. 483–490.
[6] Liu, Z., and Angeles, J., 1994, "Optimization of Planar, Spherical, and Spatial Function Generators Using Input-Output Curve Planning," J. Mech. Des., **116**(3), pp. 915–919.
[7] Primrose, E., and Freudenstein, F., 1969, "Spatial Motions 1-Point Paths of Mechanisms With Four or Fewer Links," ASME J. Eng. Ind., **91**(1), pp. 103–111.
[8] Jamalov, R., Litvin, F., and Roth, B., 1984, "Analysis and Design of RCCC Linkages," Mech. Mach. Theory, **19**(4/5), pp. 397–407.
[9] Roth, B., 2005, "Finding Geometric Invariants From Time-Based Invariants for Spherical and Spatial Motions," J. Mech. Des., **127**(2), pp. 227–231.
[10] Venanzi, S., and Parenti-Castelli, V., 2005, "A New Technique for Clearance Influence Analysis in Spatial Mechanisms," J. Mech. Des., **127**(3), pp. 446–455.
[11] Kihonge, J., Vance, J., and Larochelle, P., 2002, "Spatial Mechanism Design in Virtual Reality With Networking," J. Mech. Des., **124**, pp. 435–440.
[12] Steger, R., Lin, K., Adelstein, B., and Kazerooni, H., 2004, "Design of a Passively Balanced Spatial Linkage Haptic Interface," J. Mech. Des., **126**(6), pp. 984–991.
[13] Rajagopalan, S., and Cutkocky, M., 2003, "Error Analysis for the In Situ Fabrication of Mechanisms," J. Mech. Des., **125**(4), pp. 809–822.
[14] Marble, S., and Pennock, G., 1998, "A Study of the Coupler Curves of the RCCC Spatial Four-Bar Mechanism," *Proc. of World Congress on the Theory of Machines and Mechanisms*, Oulu, Finland, Oulu University Press, Finland, pp. 656–665.
[15] de Jager, P., Broek, J., Horvath, I., Kooijman, A., and de Smit, A., 2001, "An Effective Geometric and Kinematical Analysis of Ruled Surface Feature Manufacturability for Rapid Prototyping," *Proc. of ASME Design Engineering Technical Conference*, Pittsburgh, ASME, New York.
[16] Li, S., Ge, Q., and Varshney, A., 2001, "Web-Based Interactive Design of Freeform Motions," *Proc. of ASME Design Engineering Technical Conference*, Pittsburgh.
[17] Larochelle, P., and Agius, A., 2002, "SPASUR: Interactive Visualization of the Coupler Surfaces of the Spatial 4c Mechanism," *Proc. of ASME Design Engi-neering Technical Conference*, Montreal, Canada, ASME, New York.
[18] Duffy, J., 1980, *Analysis of Mechanisms and Robot Manipulators*, Wiley, New York.
[19] Yang, A., 1963, "Application of Quaternion Algebra and Dual Numbers to the Analyses of Spatial Mechanisms," Ph.D. Dissertation, Columbia University, New York.
[20] Murray, A. P., and Larochelle, P., 1998, "A Classification Scheme for Planar 4r, Spherical 4r, and Spatial RCCC Linkages to Facilitate Computer Anima-tion," *Proc. of ASME Design Engineering Technical Conference*, Atlanta, ASME, New York.
[21] Faux, I., and Pratt, M., 1979, *Computational Geometry for Design and Manu-facture*, Ellis Horwood, Chichester.
[22] Foster, D., and Cipra, R., 1998, "Assembly Configurations of Spatial Single-Loop Mechanisms With Revolute, Cylindric, and Prismatic Joints," *Proc. of ASME Design Engineering Technical Conference*, Atlanta, ASME, New York.
[23] Vance, J., Larochelle, P., and Dorozhkin, D., "Designing Spatial Mechanisms Using Virtual Reality," *ASME Design, Engineering Technical Conferences*, Montreal, Canada, September 29-October 2, 2002, ASME, New York.
[24] Agius, A., 2002, "Generation and Visualization of the Coupler Surfaces of Spatial 4c Mechanisms," Master's Thesis, Florida Institute of Technology.